In-Orbit Calibration and Validation of HY-2B Altimeter Using an Improved Transponder

Caiyun Wang, Mingsen Lin, Chaofei Ma, Ke Xu, Peng Liu, Te Wang, Bo Mu, Jinbiao Zhu, and Wei Guo

***Abstract*—HY-2B (Haiyang) is the follow-on mission to HY-2A, the Chinese first sea satellite for oceanography, launched in October 2018. The main payloads onboard are similar to HY-2A. For the altimeter, an in-orbit calibration mode was designed to achieve higher calibration precision. An improved transponder was built and deployed for the calibration campaign. The purpose of this article is to describe the in-orbit calibration and validation of HY-2B altimeter based on an improved transponder. A signal-rebuilt transponder was developed and employed in HY-2A altimeter calibration. It played an important role in the quantitative analysis of HY-2A altimeter data products. For HY-2B altimeter, a newly designed calibration mode was added, and an improved transponder was built. It has some advantages over the previous one in the rebuilt signal forms and modulation ways. Two calibration campaigns were carried out, in April 2019 and October 2020 at different sites. In the two campaigns, the precision of the altimeter range calibration is obtained less than 1 cm. For further validation and assessment of the result, a comparison between HY-2B and Jason-3 was performed in terms of sea surface height on the tens of cross track points in the open ocean. The comparison result shows high degree of accuracy and stability of HY-2B altimeter instrument. In China's next five-year plan (2021–2025), many more transponders and related calibration facilities would be installed in the ocean calibration fields, serving a variety of different satellite altimetry missions.**

***Index Terms*—HY-2B altimeter, improved transponder, in-orbit calibration, integration, validation.**

I. Introduction

HY-2B IS the second China's satellite for oceanic dynamic, launched in October 2018. The main payloads on HY-2B, similar to HY-2A, include a dual-frequency radar altimeter, a three-band nadir-looking radiometer for atmospheric correction, and a Ku-band radar scatterometer [1].

HY-2A has been working for over seven years. Some evaluations show the precision of sea surface height (SSH) is more than 4 cm [2]–[4]. In HY-2B, a rubidium atomic clock is first used as the frequency reference to synchronize the ultrastable oscillator (USO), therefore, the design accuracy of SSH for HY-2B is improved to 2 cm [1].

To provide truly global sea level within a geodetic system, also to obtain the altimeter instrument delay after launch, an in-orbit calibration is essential. A signal-rebuilt transponder was employed in HY-2A altimeter calibration [5], [6]. The range calibration precision of better than 2 cm was obtained, and the HY-2A USO clock drift was also estimated accurately from the calibration data [7]–[9].

In order to have a thorough test and comprehensive verification prior to its launch, a fully functional return signal simulator (RSS) was developed in our lab [10], [11]. It can provide flexible echo forms, precise time delay, and better signal-to-noise ratio, being an ideal simulator for the altimeter function test before its launch. Based on the RSS, an improved transponder was developed early in 2019, and employed in two calibration campaigns, April 2019 and October 2020, at different sites [12], [13].

Utilizing the CRS1 calibration facilities in West Crete, Greece, HY-2A altimeter SSH was assessed and compared with Jason series, SARAL/AltiKa, CryoSat-2, Sentinel-3, etc. [20], [21]. The main facilities at CRS1 are offshore GPS buoys and coastal tide gauges, which provide a direct or an extrapolated SSH *in situ*. The sea surface facilities are conventional methods used in calibration campaigns for many types of altimeters, which operate in a low-resolution mode, synthetic aperture radar mode, or interferometric synthetic aperture radar mode [14]–[25]. In recent years, inland lakes are also used for altimeter bias calibration, such as the Lake Issyk Kul in Kyrgyzstan for Jason-3 and Sentinel-3A [26].

Contrary to the sea surface facilities, the microwave transponder enables direct range measurements on land and eliminates many error sources induced by the sea surface dynamics. The existing ground-based transponders are bent-pipe ones, used in Jason-2, ERS-1/2, ENVISAT, Sentinel-3, Cryosat-2 for altimeter range bias calibration [27]–[31], [34]–[38] and backscatter coefficient sigma naught calibration [32], [33]. Bent-pipe transponder receives the altimeter signals, amplifies them, and transmits them back to the altimeter. They are simple, economical, and stable, installed at a fixed location on the satellite ground tracks, providing a constant signal delay [34], [35].

A signal-rebuilt transponder was developed and employed in HY-2A altimeter calibration, which is different from the bend-pipe ones. The bend-pipe transponder is simple and stable, but it provides constant time delay introduced by the electronic devices in the transponder [30]. Therefore, the bend-pipe transponder could be used only on a fixed position, waiting

Manuscript received April 20, 2021; revised July 15, 2021; accepted August 31, 2021. Date of publication September 13, 2021; date of current version October 15, 2021. *(Corresponding author: Mingsen Lin.)*

Caiyun Wang, Ke Xu, Peng Liu, Te Wang, and Wei Guo are with the National Space Science Center, Chinese Academy of Sciences, Beijing 100190, China (e-mail: wangcaiyun@mirslab.cn; xuke@mirslab.cn; liupeng@mirslab.cn; wangte@mirslab.cn; guowei@mirslab.cn).

Mingsen Lin, Chaofei Ma, and Bo Mu are with the National Satellite Ocean Application Service Center, Beijing 100081, China (e-mail: mslin@mail.nsoas.org.cn; mcf@mail.nsoas.org.cn; mubo@mail.nsoas.org.cn).

Jinbiao Zhu is with the Aerospace Information Research Institute, Chinese Academy of Sciences, Beijing 100094, China (e-mail: zhujb@aircas.ac.cn).

Digital Object Identifier 10.1109/JSTARS.2021.3111922

for the satellite passing over. On the contrary, the signal-rebuilt transponder can capture, track altimeter pulses, and transmit the rebuilt signals to the altimeter [5]. It is rather flexible, utilized in different positions on a mobile platform. The arrival time of the altimeter pulses at the transponder could be estimated accurately by the dechirping technique [6]. Jitters on the rising edges of the rebuilt signals are rather small by using an atomic clock in the transponder, and the inaccuracies introduced from them could be decreased greatly by averaging multiple rebuilt pulses. The rebuilt signals are not identical to the received ones. The difference between them could be eliminated from the captured pulses, in which the frequency difference between the altimeter pulses and the transponder local oscillator (L.O.) could be estimated accurately and compensated in the rebuilt signals.

For HY-2B, an improved transponder was designed and utilized in two calibration campaigns. The altimeter instrument delay is obtained, and the range calibration precision is better than 1 cm [12].

II. Improvement and Characterization of HY-2B Altimeter Transponder

A. Improvements Over the Previous Transponder

A newly designed calibration mode was added to HY-2B altimeter, in which the raw in-phase and quadrature (I/Q) data of all the odd number pulses in one burst was downloaded. Compared with HY-2A, only one pulse obtained every four bursts, the available data are greatly increased.

Based on the signal-rebuilt transponder for HY-2A and the RSS [10], [11], some improvements were done in the newly built transponder, including digital intermediate frequency (IF), direct digital synthesis (DDS), time-division frequency modulation, self-calibration, etc.

B. Characters and Performance of the Improved Transponder

The transponder captures and tracks altimeter pulses, records them, and transmits the rebuilt signals to the altimeter [5]. It provides flexible time delay and many forms of rebuilt signals. Furthermore, as a result of the capture and tracking feature, the altimeter clock drift could be derived from the calibration data [6]. The working principle is shown in Fig. 1.

HY-2B transponder consists of three main subunits: antenna, radio frequency (RF) unit, and digital control unit.

The altimeter RF pulses are received by the transponder, dechirped, and the narrow-band IF signals are obtained, which are then sampled and demodulated to digital I/Q signals. The advantage of the digital method is to achieve high phase orthogonality and amplitude consistency. After modulation and digital–analog conversion, the rebuilt signals are output to the RF transmitter.

The real transponder is shown in Fig. 2. It is carried in a truck. During experiments, the antenna is set up on a tripod, and the other electronic devices are fixed in the truck. Some auxiliary instruments are necessary. A set of static Global Navigation Satellite System (GNSS) is needed to obtain the transponder accurate geographic location and the atmospheric delay at zenith. A laser rangefinder is used to relate the GPS antenna to the transponder antenna phase center. A portable power is charged each time before experiments to supply for all the electronic devices. A portable computer (PC) is needed for parameter input, data download, and monitoring during the satellite passing over.

The main specifications of HY-2B transponder are tabulated in Table I.

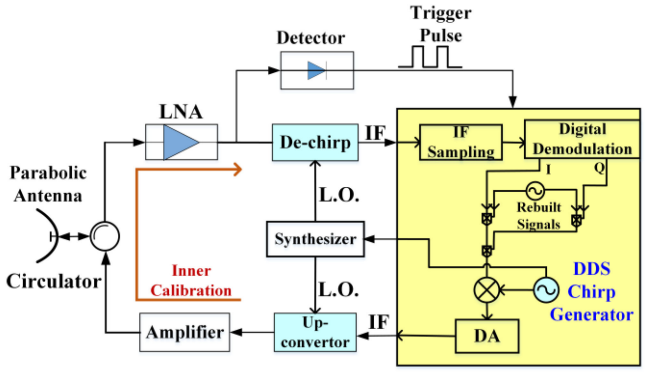

Fig. 1. Block diagram of HY-2B improved transponder.

Fig. 2. Transponder for HY-2B altimeter in calibration.

TABLE I
HY-2B Transponder Specifications

Specification	Value
Center Frequency	13.58 GHz/5.25 GHz
Received Signal Bandwidth	320/80/20 MHz
Rebuilt Signal Bandwidth	320 MHz
Transmit Power	≥1 W
Rebuilt Signal Form	Direct Digital Synthesis
Reference Clock	Rubidium Atomic Clock
Antenna	Parabolic Reflector
Polarization	Circular
Platform	Vehicle Carried
Altimetry Calibration Precision	Better than 1 cm

Fig. 3. Antenna test in a chamber.

TABLE II
ANTENNA ELECTRICAL PERFORMANCES

Specification	Value
Frequency Range	2-15 GHz
Gain	≥40 dB
First Side-lobe Level	≤-16 dB
Polarization	Dual circular
Standing-wave Ratio (SWR)	1.25
Transmit-receive Isolation	≥85 dB
Cross Polarization Isolation	≥30 dB
Pointing Precision	0.01°

C. Subunits of the Transponder

A broadband circular-polarization low sidelobe parabolic reflector antenna is employed, installed on a tripod during experiments. Its electrical performances are tested in a chamber, shown in Fig. 3. The results are listed in Table II.

The RF unit is an important part of the device, performing RF signal receiving, transmitting, down-conversion, and frequency synthesis. It includes an RF front end, an RF receive/transmit module, and a frequency synthesizer.

Two dependent channels, Ku and *C* bands, are in the front end, illustrated in Fig. 4. The received and transmitted signals are separated by a circulator. A coupler is utilized to test a portion of transmitted signals, performing the inner calibration of the transponder system. The inner calibration is performed each time before and after the satellite passing over, to monitor the variations of time delay and system gain of the transponder.

The RF receive module is to dechirp the RF signals and down-convert them to IF. The two dechirp L.O.s are at 12.48 GHz ± 160 MHz and 4.15 GHz ± 160 MHz. A switch is used to share the IF channel, as illustrated in Fig. 5. The narrow-band 1.1 GHz IF signals are down-converted to 140 MHz, and output to the digital control unit.

The RF transmit module is to up-convert the rebuilt signals to RF pulses. The rebuilt signals are generated in the digital control

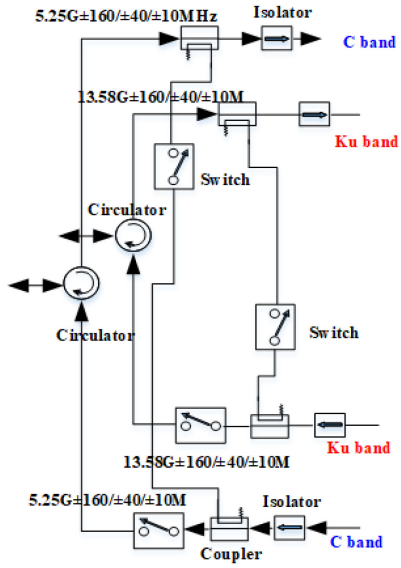

Fig. 4. Block diagram of RF front end.

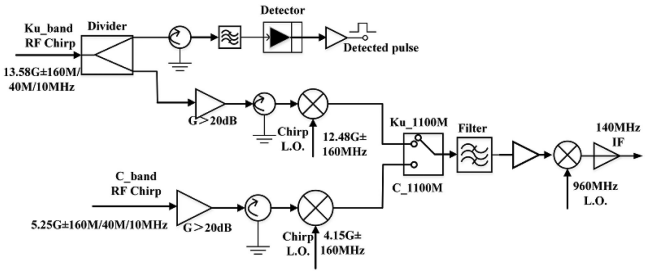

Fig. 5. Block diagram of RF receive module.

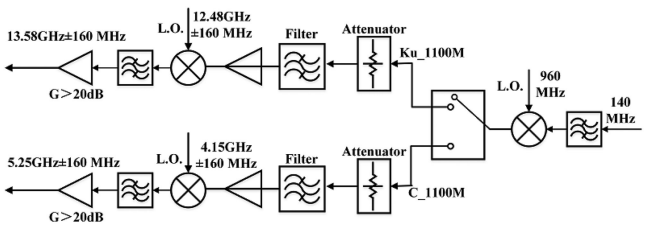

Fig. 6. Block diagram of RF transmit module.

unit, center frequency at 140 MHz. They are then up-converted to 1.1 GHz. The two transmit chirp L.O.s are 12.48 GHz ± 160 MHz and 4.15 GHz ± 160 MHz, as illustrated in Fig. 6. The RF pulses are then output to the RF front end, through the two circulators to the antenna.

A rubidium atomic clock is used in the synthesizer as the reference frequency source, to obtain high precision and stability. It generates all the required clock signals. The phase-lock loop technology and frequency doubling and mixing technologies are used in the synthesizer.

The digital control unit is the kernel of the transponder, providing the system sequential logic control and signal processing.

In HY-2B transponder, the analog quadrature modulators are replaced by digital modulators based on field-programmable

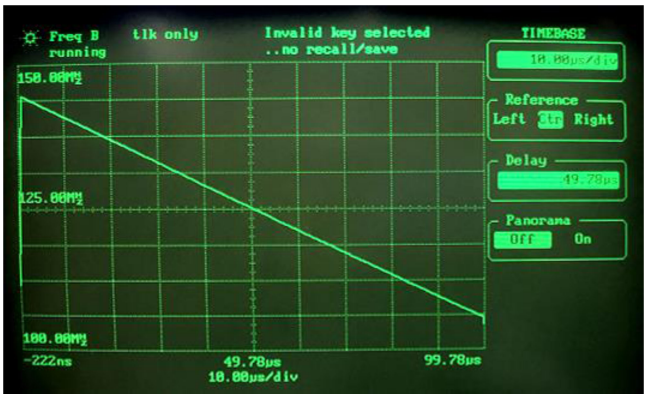

Fig. 7. Frequency linearity of DDS chirp.

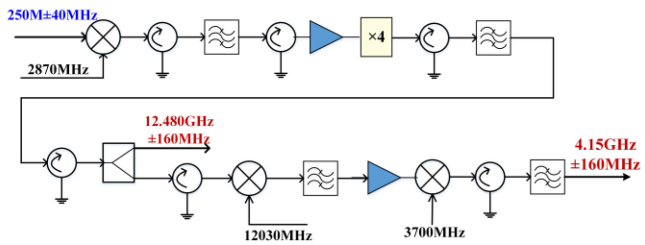

Fig. 8. Block diagram of L.O. chirps.

gate array (FPGA), obtaining a better phase quadrature and amplitude balance of the baseband I/Q signals.

The IF 140 MHz signals are demodulated and recorded in FPGA. Then the rebuilt signals are generated and modulated in frequency or time to ensure the transmitted RF signals enter the altimeter receiving windows accurately. A DDS circuit is developed in the digital control unit to generate the required chirp L.O.s. Compared with the analog method, the DDS provides a variety of rebuilt signal forms, flexible time delay, better frequency linearity, and low spurious. The DDS generated chirps are shown in Fig. 7, by a modulation domain analyzer. They are negative frequency rates. The center frequency and bandwidth are 125 and 40 MHz. Its pulsewidth is 102.4 μs. The DDS chirps are multiplied to 250 MHz $\pm$ 40 MHz, then are mixed with 2870 MHz and multiplied by four, and the 12.48 GHz $\pm$ 160 MHz L.O. are obtained. These chirps are then mixed with 12 030 MHz and 3700 MHz, and the 4.15 GHz $\pm$ 160 MHz L.O. chirps are obtained, which is illustrated in Fig. 8.

HY-2B altimeter receiving window is $\pm$60 m. For the transponder transmitted signals to enter the windows, accurate orbit prediction is essential. However, the short-term orbit prediction could have an error of dozens of meters to more than one hundred. To enable the transponder transmitted signals, enter the altimeter window accurately. A time-division frequency modulation technique is used, equivalent to extending the altimeter receiving window. The rebuilt signals are divided into four time-equal segments, each modulated at different frequencies. These are 0, 1.01, –0.17, and –1.34 MHz, as displayed in Fig. 9. Using this technique, the experiment success ratio is greatly improved.

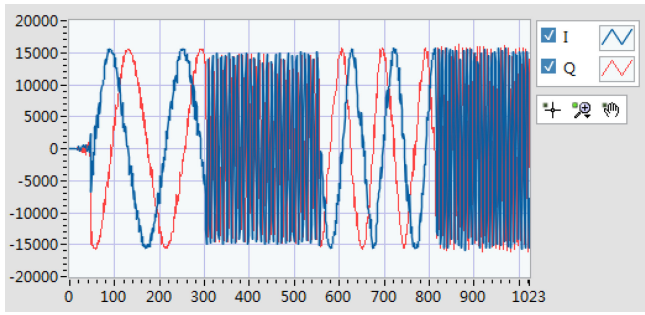

Fig. 9. Time-division frequency modulated signals.

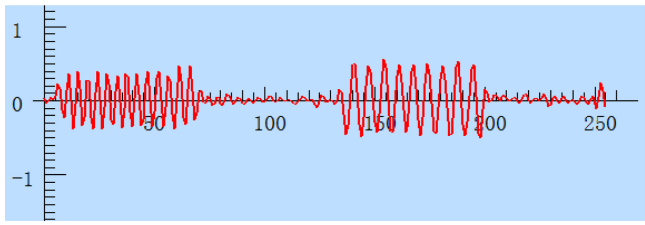

Fig. 10. Segmented echo signals received on HY-2B.

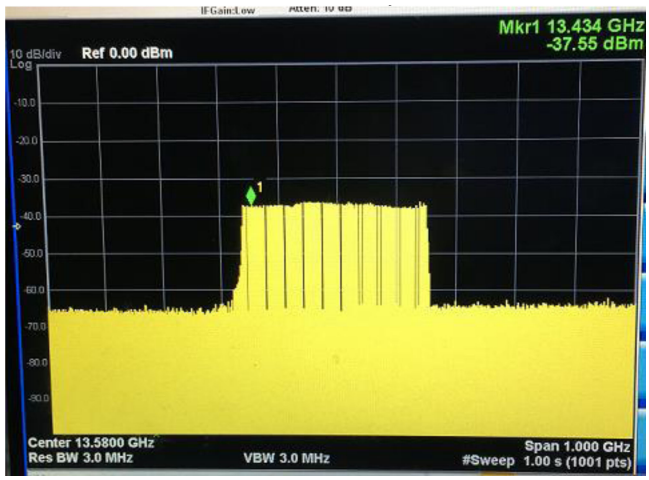

Fig. 11. Transponder rebuilt and transmitted signals spectrum.

As expected, the altimeter received echo signals are time-divided. There are two segments in the receiving window, segments one and three, shown in Fig. 10. As the satellite passes, the other segments can enter the receiving window. Using this technique, the amount of echo data is greatly increased. Therefore, the calibration precision, which heavily depends on the available echo data, is improved dramatically.

D. Integration Test and Self-Calibration

The transponder integration and test were done in our lab, using an RSS [10]. The two instruments are connected by two low loss RF cables. The RSS transmits RF pulses at the same time sequence as HY-2B altimeter, which are captured, tracked, and recorded by the transponder. Then, the transponder rebuilds pulses and transmits them back to the RSS. The transponder rebuilt signals are displayed in a spectrum analyzer, as in Fig. 11.

Fig. 12. Self-calibration of the transponder.

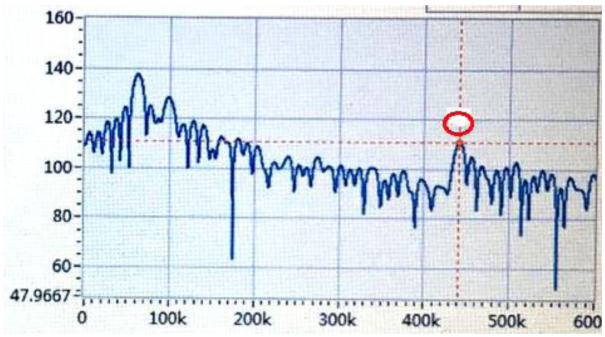

Fig. 13. Echo spectrum in self-calibration (x-axis is the number of fast Fourier transform (FFT) points, 4096 points implemented, y-axis represents the relative power of signals).

The transmitted Ku and C bands signals are 13.58 GHz±160 MHz and 5.25 GHz±160 MHz, with negative frequency rate. Its pulsewidth is 102.4 μs. The maximum power is more than 30 dBm. The transmitted power is controlled by the software installed on a portable PC. During in-orbit experiments, the output power is attenuated 10–20 dB to ensure the altimeter receiver safety.

An entire system self-calibration is essential to acquire the transponder instrument delay. It was performed by using a reflector disk installed on a delicate two-dimensional support, placed at a far distance from the transponder. The experiment was performed before the in-orbit calibration campaign, as shown in Fig. 12.

The received echoes are shown in Fig. 13, marked with a red circle. The spectrum index indicates the round distance from the transponder to the disk. The geometric distance between the transponder antenna and the disk is measured by a laser rangefinder. Subtract the geometric distance from the round, and the transponder instrument delay is obtained. Its instrument

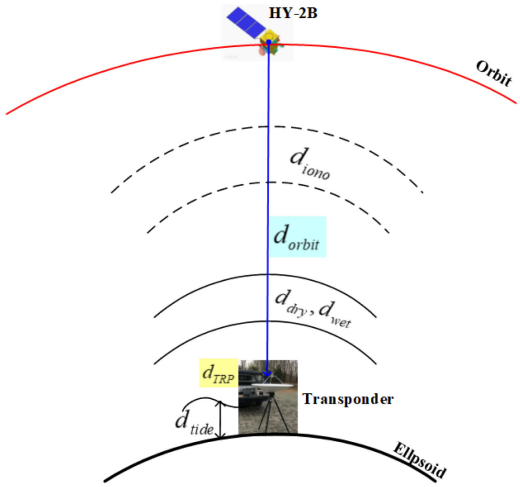

Fig. 14. Geometric relationship between altimeter and transponder.

delay is 18.81 m. The range reference point is at the end of the feed horn. During the self-calibration, an inner loop delay was recorded and was referred to as the in-orbit calibration reference. The delay of the transponder (D_TRP) measured in the Lab was used afterward in the field calibration as the transponder instrument hardware delay. If there are some modifications to the transponder hardware, another self-calibration is necessary to obtain the new D_TRP.

III. In-Orbit Calibration of HY-2B Altimeter Using the Improved Transponder

A. Principle and Methods of Calibration

The aim of the in-orbit calibration is to obtain the altimeter system delay, including instrument delay and clock drift bias. The instrument delay depends on the altimeter hardware state after the satellite was launched, which is supposed to be relevant to the instrument aging. The clock drift bias is due to the USO drift. Both these could be acquired accurately from the calibration data. The altimeter system delay could be expressed as

$$\begin{aligned} d_{\mathrm{sys}} &= d_{\mathrm{alt}} + d_{\mathrm{USO}} \\ &= (d_{\mathrm{range}} - d_{\mathrm{wet}} - d_{\mathrm{dry}} - d_{\mathrm{iono}} - d_{\mathrm{tide}} - d_{\mathrm{TRP}}) - d_{\mathrm{orbit}} \end{aligned} \quad (1)$$

where $d_{\mathrm{sys}}$is the altimeter system delay, $d_{\mathrm{alt}}$is the instrument delay, d_{USO} is the clock drift bias, d_{range} is the measured range to the transponder, including ionosphere delay, atmosphere delay, etc., and $d_{\mathrm{orbit}}$is the geometric distance from the satellite gravity center to the transponder phase center, as illustrated in Fig. 14.

In formula (1), d_{TRP} is the transponder delay, including the instrument hardware delay 18.81 m and the preset signal delay. The former's variations could be corrected by the inner calibration loop. The latter is a preset value calculated each time before the satellite passing over, according to the precise orbit prediction.

The calibration precision could be evaluated by the standard deviation (std) of the d_{alt}, which is considered a constant in a

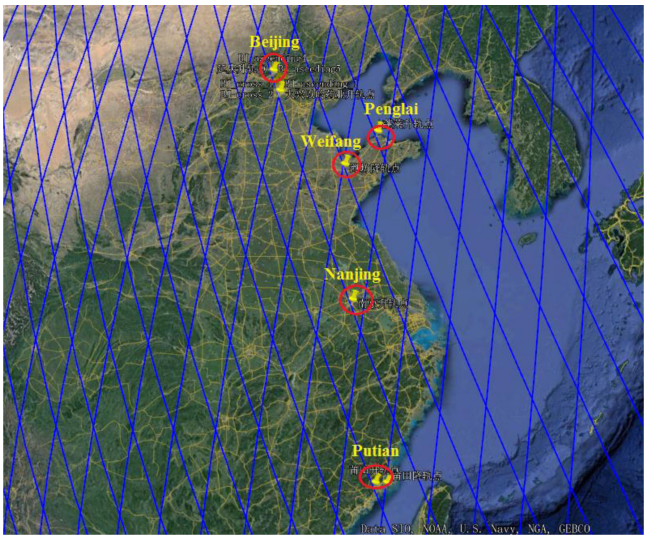

Fig. 15. Calibration sites of HY-2B altimeter in 2019.

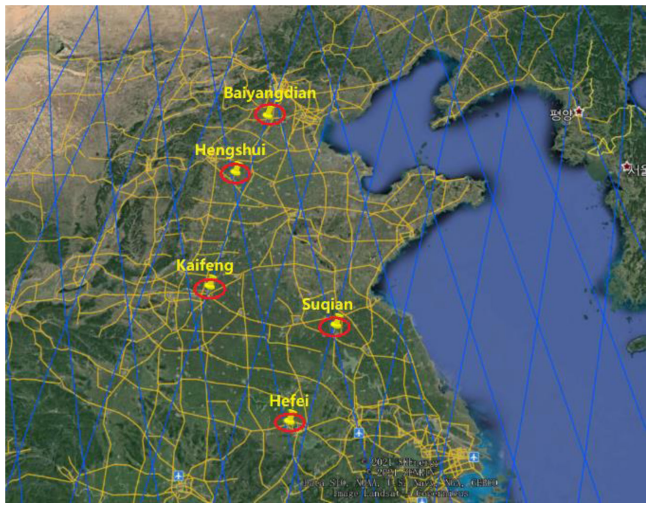

Fig. 16. Calibration sites of HY-2B altimeter in 2020.

short period. Two experiment campaigns were carried out, from April to September 2019 and October 2020. The std of $d_{\mathrm{alt}}$is obtained to be less than 1 cm in both of the two calibration campaigns. It shows that the HY-2B altimeter instrument is rather stable and the calibration results are reliable.

B. Selection of Calibration Sites

The orbit period of HY-2B is 14 days. To perform more calibration experiments in a shorter time, the transponder is designed mobile, carried on a truck.

The calibration sites were selected carefully to fulfill the following requirements.

1) It should be under, or in the proximity of the ground tracks of HY-2B, within 1 km.
2) The echo from the transponder must be stronger and distinguishable from the surrounding returns.
3) Location with high vegetation and buildings should be avoided.
4) It should be easily accessible and have little personnel activities.

A reconnaissance survey took place in April 2019 and September 2020. In total ten sites were selected. All the sites are within 300 m away from the ground tracks, being in open field, with low electromagnetic background. The locations are shown in Figs. 15 and 16, in south-east and south-central China.

The calibration sites are accurately positioned by a GNSS, listed in Table III.

Except in Beijing, one experiment was performed in the other sites. HY-2B orbit period is approximately 14 days. The reasonable selection of the calibration sites is to perform as many experiments as possible. In each 20 days of calibration campaign, April 2019 and October 2020, nine and four experiments were done separately. It is much efficient than the fix-mode calibration, once in 14 days.

TABLE III
PRECISE CALIBRATION POSITIONS IN SOUTH-EAST AND SOUTH-CENTRAL CHINA (WGS-84 COORDINATE FRAME)

Site	Longitude (°)	Latitude (°)	Height (m)
Beijing	116.249194	39.815381	47.8698
Penglai	120.679023	37.776870	102.7370
Weifang	119.058578	36.739688	24.6891
Nanjing	118.813125	31.935415	11.2843
Putian	118.850447	25.314754	117.4341
Hengshui	115.000638	38.031333	31.5648
Kaifeng	114.196482	34.761298	60.1076
Suqian	118.189972	33.958163	21.9787
Heifei	117.013392	31.730535	51.9621

C. Procedure of In-Orbit Calibration

For the accurate atmosphere correction and precise location determination of the transponder, a set of static GNSS is necessary. It was set up at least 8 h prior to the satellite passing. The GNSS antenna should be in the vicinity of 10 m to the transponder antenna.

Some preparation should be done including charging the battery, accurate orbit prediction, and calculation of the transponder rebuilt signals delay. About 30 min before the satellite passing, the transponder antenna is set up on a sturdy tripod, which is two-dimensional adjusted in azimuth and pitch. A PC is used to monitor the transponder status and download the recorded data. When the satellite passes, the transponder tracks and altimeter signals record them and rebuild the RF signals to the altimeter. Two inner calibrations are done just a few minutes before and after the passing over, recording the variations of delay and gain of the transponder instrument. The entire procedure is performed automatically, controlled by the preset program in FPGA.

HY-2B orbit height is 970 km. Its beam width is 1.1° [1], so the overhead time is about 2–3 s. After passing over, the antenna, the GPS, as well as the battery, etc., are collected and put in the truck. The procedure in one experiment is shown in Fig. 17.

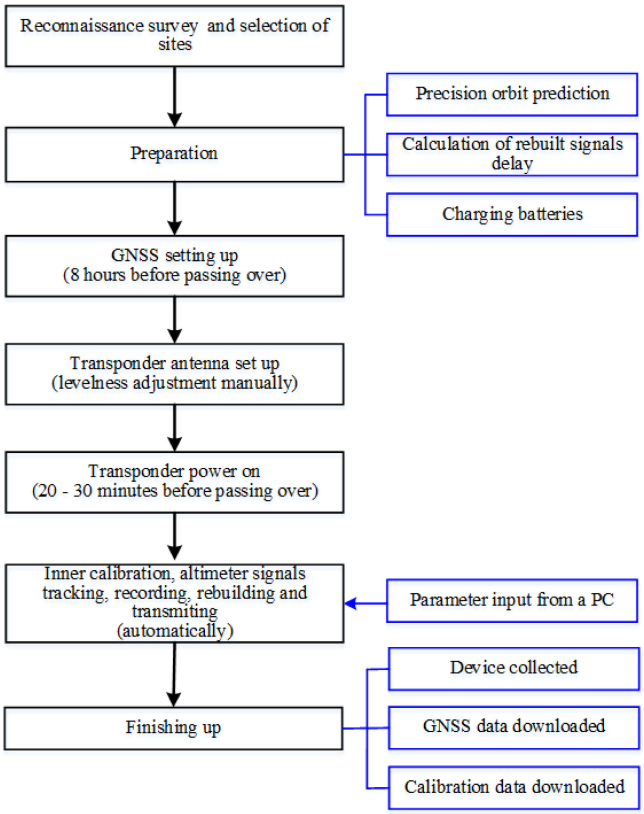

Fig. 17. In-orbit calibration experiment procedure.

Fig. 18. HY-2B in-orbit calibration experiment scenario.

Because of the narrow bandwidth of HY-2B antenna and the transponder antenna, the accurate pointing between the two is crucial. HY-2B altimeter is nadir-looking. The transponder antenna must be pointing straight upwards. This is achieved by a high precision electronic level meter. It is placed on the antenna feeder plane, which is perpendicular to the antenna electric axis by the mechanical technique. Its vertical error is less than 0.1°. The experimental scenario and antenna leveling adjustment are displayed in Figs. 18 and 19.

Fig. 19. Electronic level meter used in experiment.

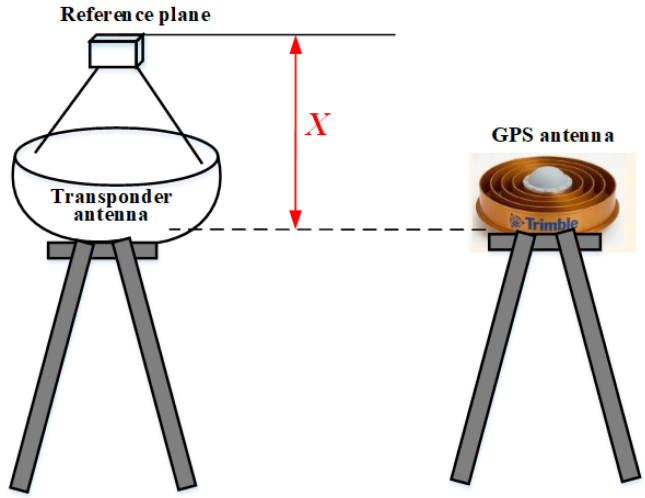

Fig. 20. Transponder geodetic height determined by GNSS.

The geodetic height of the transponder antenna phase center is determined by the static GNSS, the height that is referred to the bottom of the choke ring, and the transponder height reference is at the feeder plane; therefore, a laser level meter is utilized to correlate the GNSS geodetic height and the transponder reference plane, as illustrated in Fig. 20. The height difference X is measured accurately by a laser level meter in every experiment.

The GNSS antenna was set up at least 8 h before the satellite passing. To acquire the accurate position of the transponder, data from multiple GNSS fiducial stations as well as land state network are utilized, and the vertical precision of less than 1 cm could be obtained.

D. Calibration Data Processing and Key Techniques

A special calibration mode was designed on HY-2B, in which the raw I/Q data of all the odd number pulses in one burst was downloaded, so the available calibration data are greatly increased. It is essential to improve the calibration precision. The downloaded data are indicated in Fig. 21.

Calibration data processing is complicated. It includes the following steps.

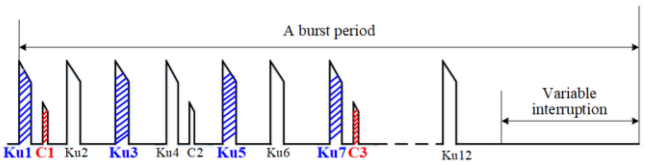

Fig. 21. Indication of HY-2B downloaded odd number pulses in one period.

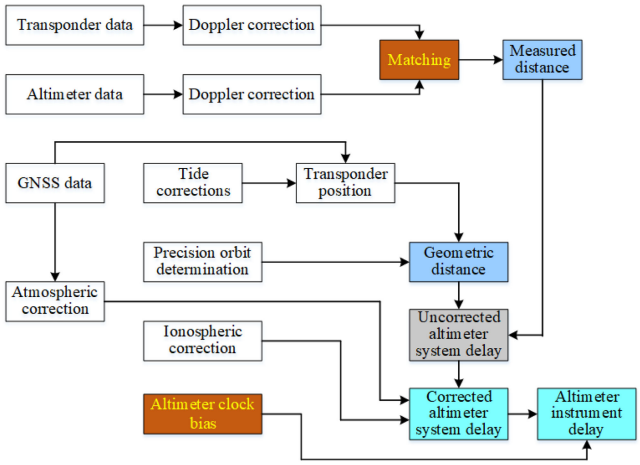

Fig. 22. Flowchart of transponder calibration developed for HY-2B altimeter instrument delay estimation.

1) The time-frequency domain conversion of the transponder data and the altimeter data.
2) The accurate matching between the altimeter and the transponder pulses.
3) Obtaining the measured range from the altimeter data.
4) Obtaining the geometric distance from the precise orbit determination (POD) file and the GNSS data.
5) Correction to the measured range, including Doppler correction, propagation delay correction, transponder delay correction, tide correction, etc.
6) Obtaining the altimeter system delay, including the clock drift bias and the instrument delay.
7) Subtracting the clock drift bias, obtaining the altimeter instrument delay.

The procedure is described in Fig. 22.

The key techniques in the data processing are the altimeter-transponder pulse matching and the altimeter clock bias correction. The method to estimate HY-2B altimeter clock drift is similar to HY-2A [6], [7]. In HY-2B, a rubidium atomic clock is used [1]. It is rather stable, with very small long-term drift.

Establishing correspondence between altimeter data and transponder data is the first and crucial step in processing. A new method based on shape match of the FFT waveforms of the altimeter and transponder data is used. According to the principle of the dechirping, the transponder data are displayed in Fig. 23. On the contrary, the altimeter data are as shown in Fig. 24. Their spectrums exhibit approximate mirror symmetry.

The abscissa of the maximum power in the FFT spectrum represents the time difference (or frequency difference) of the rising ends between the altimeter and the transponder pulses.

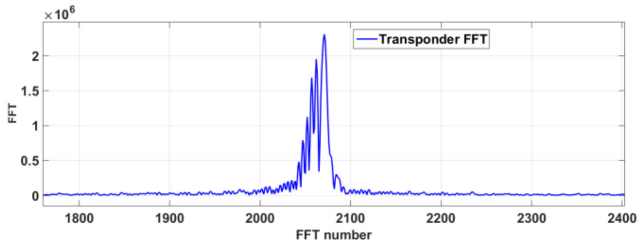

Fig. 23. Transponder data FFT waveform (*x*-axis is the number of FFT points, 4096 points implemented, *y*-axis represents the relative power of signals).

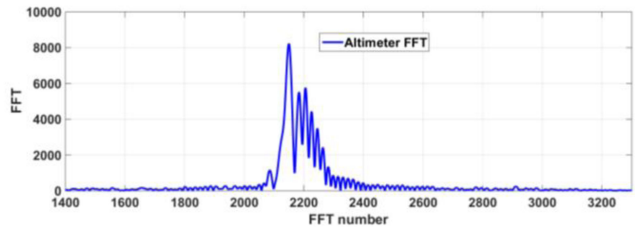

Fig. 24. Altimeter data FFT waveform (*x*-axis is the number of FFT points, 4096 points implemented, *y*-axis represents the relative power of signals).

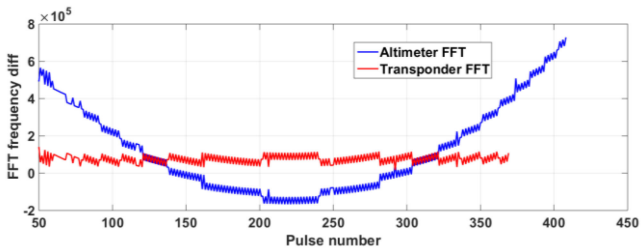

Fig. 25. Corresponding relationship between altimeter and transponder (*x*-axis is the recorded pulse number, *y*-axis represents the FFT frequency difference).

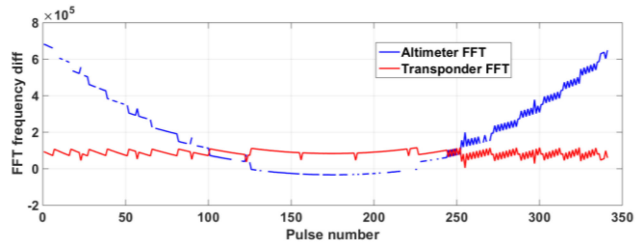

Fig. 26. Corresponding relationship between altimeter and transponder with some data missing (*x*-axis is the recorded pulse number, *y*-axis represents the FFT frequency difference).

In every successful experiment, about two or three hundreds of valid pulses are recorded and transferred in FFT. Therefore two sequences of frequency differences are obtained. For the frequency difference is included in the transponder rebuilt signals, the sequences of the altimeter and the transponder exhibit a similar shape, but in an opposite direction. Based on the shape characteristic matching, the corresponding relationship between the altimeter and the transponder would be established. The matched forms of the two sequences are shown in Figs. 25 and 26. In Fig. 26, there is a little amount of data missing because

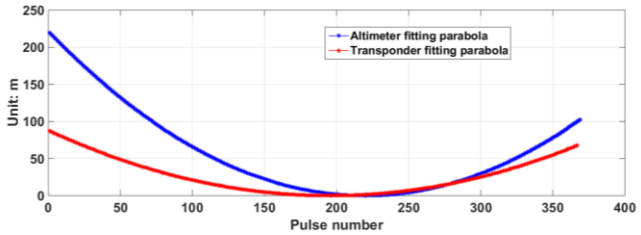

Fig. 27. Parabola fitted from the raw transponder data and the altimeter data (*x*-axis is the recorded pulse number, *y*-axis represents the pulse interval, converted to range, blue one is altimeter transmit–receive interval, red one is transponder receive–receive interval).

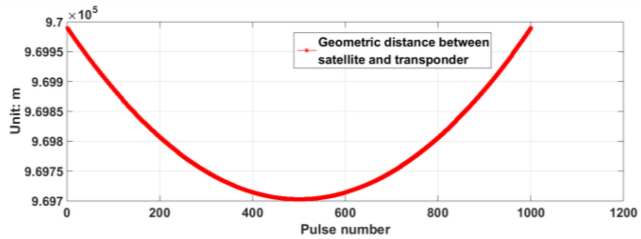

Fig. 28. Geometric distance between altimeter and transponder during passing over (*x*-axis is the recorded pulse number, *y*-axis represents the ranges).

of tracking lost or spur noises, and the shape matching method is still valid in this case.

According to the relationship between the satellite-transponder geometric distance and the timing sequence of the pulses [29], [30], the point target response of the transponder moves all along the altimeter range window resulting in a typical parabolic signature, as shown in Fig. 27. The blue curve presents the response of the transponder in the altimeter. The red one is the transponder measured one-way range changes relative to the closest approach. In the case of the clock synchronization of the satellite and the transponder, the vertices of the two parabolas would be coincidence. Therefore, according to the vertices deviation, the clock bias between the satellite and the transponder could be acquired. The method of estimating the altimeter clock drift was described in [6], [7].

The POD file is obtained one day after the satellite passes over. It is a 1-min timescale file. To match the altimeter transmit–receive time sequence, a Hermite interpolation method is used. A 16-min data is cut from the POD file, covering 8 min before and after the overhead epoch. The interpolated geometric distance between the satellite and the transponder during the passing over is shown in Fig. 28.

IV. Calibration Results and Comparison With Jason-3 on Cross Track Points

A. Calibration Results of HY-2B Altimeter

The aim of the two calibration campaigns based on the improved transponder is to obtain HY-2B altimeter instrument delay and estimate its clock drift bias. The results show that the altimeter instrument is very stable. The onboard atomic clock is rather accurate. Its drift is almost negligible.

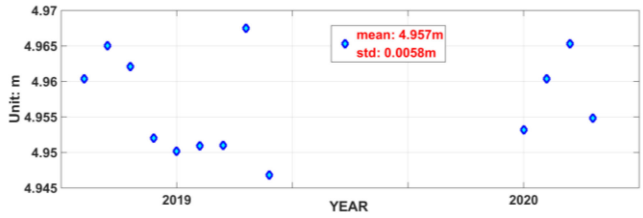

Fig. 29. HY-2B altimeter instrument delay from in-orbit calibration experiments.

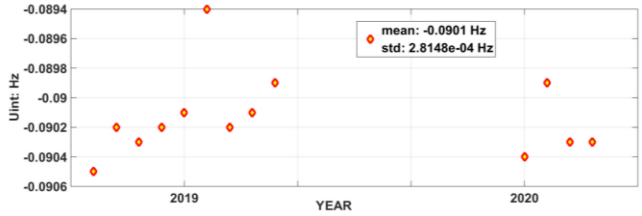

Fig. 30. HY-2B altimeter clock drift bias from in-orbit calibration experiments.

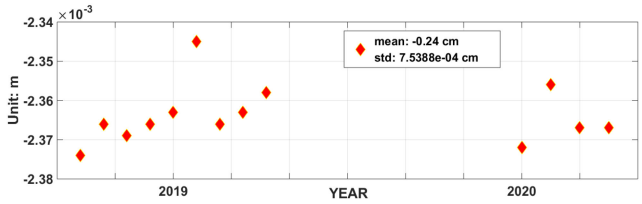

Fig. 31. Range drift introduced by clock drift.

In the two calibration campaigns April 2019 and October 2020, 13 successful experiments were done, 9 in 2019, and 4 in 2020. The mean of the altimeter instrument delay is 4.957 m, and the std is 0.68 cm, as shown in Fig. 29.

The clock drift is displayed in Fig. 30. It presents a good stability in the two years of operation. The mean bias is less than 0.1 Hz. Its std is less than 0.001 Hz. The center frequency of the clock is 80 MHz. An important parameter is DF/F0 where DF is the std deviation and F0 is the center frequency. From the obtained results, the parameter DF/F0 is less than 10^{-11}, which provides a best proof that HY-2B is much accurate and stable than HY-2A for the improvement of the clock from the oven-controlled crystal oscillator to the rubidium atomic clock.

The range drift linked to the clock drift is shown in Fig. 31. Its mean value is less than 0.5 cm and the std is less than 10^{-3} cm, which means the range drift introduced by the clock drift is rather small.

B. Comparison With Jason-3 on Cross Track Points

HY-2B altimeter tracking bias to SSH is 14.508 m. Its instrument delay is 4.957 m. Therefore, the total correction of SSH is

$$14.508 + 4.957 = 19.465 \text{ m}.$$

For the further validation, the corrected SSH acquired from HY-2B Interim Geophysical Data Record data is compared with Jason-3 at the cross track points in the open ocean on the Pacific

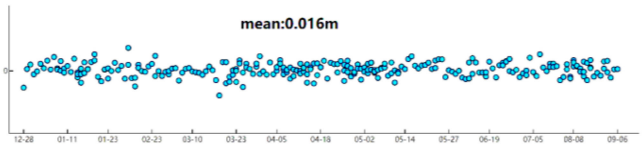

Fig. 32. Comparison of SSH between HY-2B and Jason-3 on cross track points from December 2019 to September 2020.

and the Atlantic. The time window is 5 min and the distance window is 5 km. The comparison results are shown in Fig. 32. The mean of the SSH difference is 0.016 m.

The high degree of consistency on the cross track points provides a best validation that HY-2B altimeter measurements are accurate and stable, and the calibration method based on the improved transponder is reliable and effective.

V. Conclusion

An improved transponder was developed and employed in HY-2B altimeter in-orbit calibrations in 2019 and 2020. It offers a reliable and efficient approach to obtain the altimeter's instrument delay accurately. Furthermore, it provides a special method to monitor the long-term drift of the altimeter clock. The calibration and validation results show that HY-2B altimeter is rather stable and accurate in the SSH measurement. By utilizing a rubidium atomic clock, HY-2B clock drift is decreased significantly. It presents a good performance on long-term stability. In the following Haiyang series missions, HY-2C, launched in October 2020, and HY-2D, would be launched in May 2021, the transponders would be modified and improved further to meet the new calibration requirements and adapt to the different types of signals forms. With the construction of the Chinese first ocean calibration field in Wanshan islands, calibration infrastructure is under rapid development. In China's next five-year plan (2021–2025), many more transponders and related calibration facilities would be installed in the ocean calibration field, serving a variety of different satellite altimetry missions. With the infrastructure construction and the cooperation of multiple types of calibration devices, more accurate and a wider variety of calibration and validation achievements would be achieved.

Acknowledgment

The authors would like to thank the National Satellite Ocean Application Service Center for providing HY-2B Level 0 data and Interim Geophysical Data Record data, the HY-2B altimeter payload group for assistance in the development of the improved transponder, and the in-orbit calibration campaigns.

References

[1] K. Xu, P. Liu, Y. Tang, and X. Yu, "The improved design for HY-2B radar altimeter," in *Proc. Int. Geosci. Remote Sens. Symp.*, Fort Worth, TX, USA, Jul. 2017, pp. 534–537.

[2] M. Jiang, K. Xu, X. Xu, L. Shi, X. Yu, and P. Liu, "Range noise level estimation of HY-2B radar altimeter and its comparison with Jason-2 and Jason-3 altimters," in *Proc. Int. Geosci. Remote Sens. Symp.*, Yokohama, Japan, Jul. 2019, pp. 8312–8315.

[3] M. Jiang, K. Xu, Y. Jia, C. Fan, and X. Xu, "Evaluation of HY-2B altimeter products over ocean," in *Proc. Int. Geosci. Remote Sens. Symp.*, Waikoloa, HI, USA, Sep./Oct. 2020, pp. 5858–5861.

[4] M. Jiang, K. Xu, Y. Liu, and L. Wang, "Estimating the sea state bias of HY-2A radar altimeter by a three-dimensional nonparametric model," in *Proc. Int. Geosci. Remote Sens. Symp.*, Beijing, China, Jul. 2016, pp. 396–399.

[5] C. Y. Wang, W. Guo, F. Zhao, and J. Z. Wan, "In-orbit calibration of HY-2A altimeter using a signal reconstructive transponder," in *Proc. Int. Geosci. Remote Sens. Symp.*, Quebec, QC, Canada, Jul. 2014, pp. 5119–5122.

[6] C. Wang *et al.*, "Development of the reconstructive transponder for in-orbit calibration of HY-2 altimeter," *IEEE J. Sel. Topics Appl. Earth Observ. Remote Sens.*, vol. 9, no. 6, pp. 2709–2719, Jun. 2016.

[7] J. Wan, W. Guo, F. Zhao, C. Y. Wang, and P. Liu, "HY-2A radar altimeter ultrastable oscillator drift estimation using reconstructive transponder with its validation by multi-mission cross calibration," *IEEE Trans. Geosci. Remote Sens.*, vol. 53, no. 9, pp. 5229–5236, Sep. 2015.

[8] J. Wan *et al.*, "Echo signal quality analysis during HY-2A radar altimeter calibration campaign using reconstructive transponder," *IEEE J. Sel. Topics Appl. Earth Observ. Remote Sens.*, vol. 9, no. 6, pp. 2702–2708, Jun. 2016.

[9] J. Z. H. Wan, W. Guo, C. Y. Wang, and F. Zhao, "A matching method for establishing correspondence between satellite radar altimeter data and transponder data generated during calibration," *IEEE Geosci. Remote Sens. Lett.*, vol. 11, no. 12, pp. 2145–2149, Dec. 2014.

[10] W. Guo, C. Wang, and P. Liu, "Development and pre-launch test of a return signal simulator for HY-2B altimeter," in *Proc. Int. Geosci. Remote Sens. Symp.*, Valencia, Spain, Jul. 2018, pp. 1602–1605.

[11] C. Wang, W. Guo, S. Yang, and P. Liu, "Development and performance analysis of a fully functional return signal simulator for HY-2B scatterometer," in *Proc. Int. Geosci. Remote Sens. Symp.*, Valencia, Spain, Jul. 2018, pp. 9168–9171.

[12] C. Wang, W. Guo, P. Liu, T. Wang, and H. Cui, "In-orbit calibration and validation of HY-2B altimeter using an improved transponder," in *Proc. Int. Geosci. Remote Sens. Symp.*, Waikoloa, HI, USA, Sep./Oct. 2020, pp. 5819–5822.

[13] C. Wang, W. Guo, P. Liu, and T. Wang, "Development and integration test of an improved transponder for HY-2B altimeter," in *Proc. Int. Geosci. Remote Sens. Symp.*, Waikoloa, HI, USA, Sep./Oct. 2020, pp. 5862–5865.

[14] M. Roca *et al.*, "RA-2 absolute range calibration," in *Proc. Envisat Validation Workshop*, Frascati, Italy, Dec. 9–13, 2002.

[15] D. J. Wingham *et al.*, "CryoSat: A mission to determine the fluctuations in earth's land and marine ice fields," *Adv. Space Res.*, vol. 37, no. 4, pp. 841–871, 2006, doi: 10.1016/j.asr.2005.07.027.

[16] S. P. Mertikas, A. Papadopoulos, and E. C. Pavlis, "An alternative procedure for the estimation of the altimeter bias for the Jason-1 satellite using the dedicated calibration site at Gavdos," *Proc. SPIE*, vol. 7105, Oct. 2008, Art. no. 71050H.

[17] S. P. Mertikas *et al.*, "Recent developments for the estimation of the altimeter bias for the Jason-1 and 2 satellites using the dedicated calibration site at Gavdos," *Proc. SPIE*, vol. 7473, Sep. 2009, Art. no. 74730C.

[18] S. P. Mertikas *et al.*, "Absolute calibration of Jason satellite radar altimeters at Gavdos Cal/Val facility using independent techniques," *Proc. SPIE*, vol. 7825, Oct. 2010, Art. no. 78250C.

[19] F. Frappart *et al.*, "Preliminary result of the 2013 Ibiza calibration campaign of Jason 2 and Saral altimeter," in *Proc. Int. Geosci. Remote Sens. Symp.*, Quebec, QC, Canada, Jul. 2014, pp. 4473–4476.

[20] S. P. Mertikas *et al.*, "First preliminary results for the absolute calibration of the Chinese HY-2 altimetric mission using the aCRS1 calibration facilities in West Crete, Greece," *Adv. Space Res.*, vol. 57, no. 1, pp. 78–95, 2016, doi: 10.1016/j.asr.2015.10.01. [Online]. Available: www.elsevier.com/locate/asr

[21] S. P. Mertikas *et al.*, "Gavdos/West Crete Cal/Val site: Over a decade calibrations for Jason series, SARAL/AltiKa, Cryosat-2, Sentinel-3 and HY-2 altimeter satellites," in *Proc. ESA Living Planet Symp.*, Prague, Czech Republic, vol. 740, May 9–13, 2016, p. 87.

[22] P. L. Vu *et al.*, "Multi-Satellite altimeter validation along the French Atlantic coast in the Southern Bay of biscay from ERS-2 to SARAL," *Remote Sens.*, vol. 10, pp. 93–125, 2018, doi: 10.3390/rs10010093.

[23] P. Bonnefond *et al.*, "Calibrating the SAR SSH of Sentinel-3A and Cryosat-2 over the Corsica facilities," *Remote Sens.*, vol. 10, 2018, Art. no. 92, doi: 10.3390/rs10010092.

[24] J. Yang and J. Zhang, "Validation of Sentinel-3A/3B satellite altimetry wave heights with buoy and Jason-3 data," *Sensors (Basel)*, vol. 19, no. 13, Jul. 2019, Art. no. 2914, doi: 10.3390/s19132914.

[25] Z. Wanlin, Z. Jianhua, X. Fan, L. Yan, C. Chen, and Z. Tian, "Preliminary calibration results for Jason-3 and Sentinel-3 altimeters in the Wanshan Islands," *J. Oceanol. Limnol.*, vol. 39, pp. 458–471, 2021, doi: 10.1007/s00343-020-9251-1.
[26] J.-F. Crétaux *et al.*, "Absolute calibration or validation of the altimeters on the Sentinel-3A and the Jason-3 over Lake Issykkul (Kyrgyzstan)," *Remote Sens.*, vol. 10, 2018, Art. no. 1679, doi: 10.3390/rs10111679.
[27] R. J. Powell, "Relative vertical positioning using ground-level transponders with the ERS-1 altimeter," *IEEE Trans. Geosci. Remote Sens.*, vol. GRS-24, no. 3, pp. 421–425, May 1986.
[28] A. R. Birks, "Radar altimeter calibration using ground based transponders," in *Proc. Envisat Symp.*, Montreux, Switzerland, Apr. 2000, pp. 23–27.
[29] E. Cristea and P. Moore, "Altimeter bias determination using two years of transponder observations," in *Proc. Envisat Symp.*, Montreux, Switzerland, Apr. 2007, pp. 23–27.
[30] W. Hausleitner *et al.*, "A new method of precise Jason-2 altimeter calibration using a microwave transponder," *Mar. Geodesy*, vol. 35, no. 1, pp. 337–362, Dec. 2012.
[31] A. Garcia-Mondejar *et al.*, "Sentinel-3 transponder calibration results," in *Proc. Ocean Surf. Topography Sci. Team Meeting*, Miami, FL, USA, Oct. 23–27, 2017, doi: 10.13140/RG.2.2.14938.64966.
[32] N. Pierdicca *et al.*, "Transponder calibration of the Envisat RA-2 altimeter Ku band sigma naught," *Adv. Space Res.*, vol. 51, pp. 1478–1491, 2013.
[33] N. Pierdicca *et al.*, "Transponder calibration of the ENVISAT RA-2 altimeter sigma naught," in *Proc. Int. Geosci. Remote Sens. Symp.*, Munich, Germany, Jul. 2012, pp. 2675–2678.
[34] S. P. Mertikas *et al.*, "Fifteen years of Cal/Val service to reference altimetry missions: Calibration of satellite altimetry at the permanent facilities in Gavdos and Crete, Greece," *Remote Sens.*, vol. 10, 2018, Art. no. 1557, doi: 10.3390/rs10101557.
[35] S. Mertikas *et al.*, "A permanent infrastructure in Crete for the calibration of Sentinel-3, Cryosat-2 and Jason missions with transponder," in *Proc. ESA Living Planet Symp.*, Edinburgh, U.K., Sep. 9–13, 2013, p. 10.
[36] S. P. Mertikas *et al.*, "Absolute calibration of the Sentinel-3 altimeter with sea-surface and transponder at FRM standards in West Crete, Greece," in *Proc. Int. Rev. Workshop Satell. Altimetry Cal/Val Activities Appl.*, vol. 10, no. 11, Chania, Greece, Apr. 23–26, 2018, Art. no. 1808, doi: 10.3390/rs10111808.
[37] S. Mertikas *et al.*, "Absolute calibration of the European Sentinel-3A surface topography mission over the permanent facility for altimetry calibration in West Crete, Greece," *Remote Sens.*, vol. 10, 2018, Art. no. 1808, doi: 10.3390/rs10111808.
[38] S. Mertikas *et al.*, "The ESA permanent facility for altimetry calibration monitoring performance of radar altimeters for Sentinel-3A, Sentinel-3B and Jason-3 using transponder and sea-surface calibrations with FRM standards," *Remote Sens.*, vol. 12, 2020, Art. no. 2642, doi: 10.3390/rs12162642.
[39] M. B. Mathews, "Design, testing, and performance analysis of transponders for use with satellite altimeters," Ph.D. dissertation, Univ. Colorado Boulder, Boulder, CO, USA, 1995.
[40] R. Touzi, R. K. Hawkins, and S. Côté, "High-Precision assessment and calibration of polarimetric RADARSAT-2 SAR using transponder measurements," *IEEE Trans. Geosci. Remote Sens.*, vol. 51, no. 1, pp. 487–503, Jan. 2013.

Caiyun Wang received the B.Eng. and M.Eng. degrees in communication and information engineering from Xidian University, Xi'an, China, in 1997 and 2001, respectively.

She is currently an Associate Professor with the Nation Space Science Center, Chinese Academy of Sciences, Beijing, China. Her research interests include calibration and validation of satellite-borne altimeter, synthesized aperture radar and scatterometer.

Mingsen Lin was born in Fujian, China, in 1963. He received the Ph.D. degree from the Computing Center of Chinese Academy of Sciences, Beijing, China, in 1992.

He is currently a Professor with the National Satellite Ocean Application Center, Beijing, China. His research interests include microwave remote sensing of ocean wind, ocean satellite data processing algorithm, and ground-based observations.

Chaofei Ma was born in Hunan, China, in 1971. He received the Ph.D. degree from the Institute of Remote Sensing Applications, Chinese Academy of Sciences, Beijing, China, in 2002, and mainly engaged in Cal/Val of China Ocean Satellites.

He is responsible for the calibration and validation of the Haiyang Satellite. He is also the main participant of the Haiyang Satellite ground systems construction and on-orbit operation.

Ke Xu is a Professor with the National Microwave Remote Sensing Laboratory, Chinese Academy of Sciences, Beijing, China. He is the Chief Designer for the HY-2A/B/C satellite radar altimeter. His research interests include space-borne radar altimeter design, synthetic aperture radar altimeter, and signal processing.

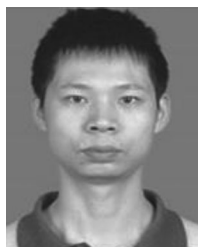

Peng Liu was born in Hunan, China, in 1983. He received the Ph.D. degree from the University of Chinese Academy of Sciences (CAS), Beijing, China, in 2018.

He is a Senior Engineer with the National Space Science Center, CAS. His research interests include high-speed digital signal processing, FPGA programming, system integration and test.

Te Wang was born in Hunan, China, in 1989. He received the M.D. degree from Beijing University of Technology, Beijing, China, in 2014.

He is a Senior Engineer with the Nation Space Science Center, Chinese Academy of Sciences, Beijing, China. He is engaged in the software development and data processing. He is one of the main participants in the HY-2B altimeter in-orbit calibration missions.

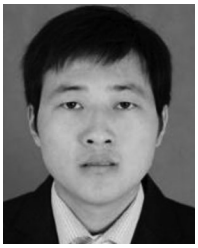

Bo Mu was born in Shaanxi, China, in 1985. He received the M.D. degree from the National Marine Environmental Forecasting Research Center, Beijing, China, in 2010.

His research interests include active microwave remote sensor calibration and validation, *in situ* measurements technology, and data applications. He is now the main participant of the HY-2A/B/C Satellite ground systems construction and on-orbit operation.

Jinbiao Zhu was born in Shandong, China, in 1977. He received the M.D. degree from Tsinghua University, Beijing, China, in 2018.

He is a Professor of engineering with the Aerospace Information Research Institute, Chinese Academy of Sciences, Beijing, China. He is engaged in the airborne remote sensing technologies and applications.

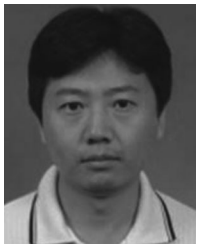

Wei Guo received the Ph.D. degree from the Institute of Electronics, Chinese Academy of Sciences (CAS), Beijing, China, in 1999.

From 1999 to 2001, he did postdoctoral work in sea surface returned signal simulator development for radar altimeter calibration with the National Space Science Center, CAS. His current research focuses on the calibration of HY-2 satellite altimeter by using reconstructive transponder. He is the primary investigator of the signal reconstructive transponder.